Laminar forced convection of power-law fluids in the entrance region of parallel plates ducts

CrossMark

Damián Crespí-Llorens [a,*], Nicolas Galanis [b]

[a] Dep. Ing. Mecánica y Energía, Universidad Miguel Hernández de Elche, Av. de la Universidad s/n, 03202 Elche, Spain
[b] Génie mécanique, Université de Sherbrooke, Sherbrooke, QC J1K2R1, Canada

A B S T R A C T

An approximate analytical solution for forced convection of power-law fluids in the entrance region of parallel-plates ducts with the uniform heat flux boundary condition (H condition) is presented and analyzed. It is based on the assumption of similarity between the profiles of the velocity and the temperature in the respective boundary layers and in the fully developed region where exact analytical profiles are obtained from the differential conservation equations. The axial evolutions of the hydrodynamic and thermal boundary layers, of the pressure loss, of the skin friction coefficient and of the Nusselt number are also obtained by applying the integral form of the conservation equations in the entrance region. For a flow behavior index equal to unity (Newtonian fluid) the predicted values of these parameters are in good agreement with corresponding data from the literature.

© 2017 Published by Elsevier Ltd.

1. Introduction

Many fluids in the food and petrochemical industries are non-Newtonian. In such applications the determination of parameters such as the friction factor and the Nusselt number is necessary for the calculation of pressure losses and heat transfer rates or temperature distributions. This can be achieved either experimentally or theoretically by solving the appropriate transport equations for typical common geometries (circular ducts, flat ducts, etc.). An important characteristic of these fluids is that they have large apparent viscosities. Therefore, laminar flow conditions occur more often than with Newtonian fluids.

In this paper we analyze the steady-state developing laminar flow of a power-law fluid with constant properties within a parallel-plates duct.

For Newtonian fluids this problem has been solved by several investigators for uniform wall temperature (T condition) and uniform heat flux (H condition). The hydrodynamically developing isothermal flow was solved numerically by Bodoia & Osterle [1] and analytically by Bhatti & Savery [2]. The corresponding thermal entrance problem was solved analytically by Sparrow et al. [3] for the H condition and by Nusselt, Graetz and Lévêque [4] for the T condition. Their expressions for the temperature and Nusselt numbers are given in [4]. According to Shah & Bhatti [4] the most accu-

rate results for the simultaneously developing flow with both thermal boundary conditions are those of a numerical study by Hwang & Fan [5] who presented them in tabular form. For $Pr = 0$ (slug flow) exact analytical expressions for the temperature distribution and the local and average Nusselt numbers are given in [4].

For non-Newtonian fluids this problem has been often studied for isothermal flows. It has also been addressed for forced convection with uniform constant wall temperature (T condition). Thus, Yau & Tien [6] applied the momentum and energy integral method to determine the simultaneous development of velocity and temperature profiles for a constant property fluid obeying the Ostwald-de Waels model (power law). The inlet temperature and velocity profiles were assumed uniform and they obtained approximate expressions for the non-dimensional temperature, velocity and pressure drop as well as for the Nusselt number. The values of the constants appearing in these expressions depend on the flow behavior index and were determined numerically but are not included in [6]. It should be noted that at $x = L_{hy}$ the approximate velocity profile determined by Yaw & Tien does not match the exact analytically determined fully developed velocity profile. Richardson [7] extended the Lévêque solution for hydrodynamically developed flow in ducts with constant wall temperature for the case of a power law fluid. The effect of heat generation by viscous dissipation was included. Matras & Nowak [8] developed a transformation method which converts the isothermal flow of a power-law fluid to an equivalent pseudo-Newtonian flow. They then used the momentum integral method to solve the

* Corresponding author.
 E-mail address: dcrespi@umh.es (D. Crespí-Llorens).

Nomenclature

b	half-distance between plates [m]
C_f	skin friction coefficient
c_p	specific heat [J kg^{-1} K^{-1}]
D_h	hydraulic diameter, $D_h = 4b$ [m]
k	conductivity [W m^{-1} K^{-1}]
L_{hy}, L_{th}	hydrodynamic, thermal development lengths [m]
L_{hy}^*	non-dimensional hydrodynamic entrance length, $L_{hy}^* = L_{hy}/(D_h Re)$
$\widehat{L}_{th}$	non-dimensional thermal entrance length, $\widehat{L}_{th} = L_{th}/(D_h Re Pr)$
m	fluid consistency coefficient [Pa s^n]
$\dot{m}$	mass flowrate [kg s^{-1}]
n	flow behavior index
P	pressure [Pa]
P^*	non-dimensional pressure, $P^* = (P_0 - P(x))/(0.5\rho U_0^2)$
Pr	Prandtl number, $Pr = c_p m U_0^{n-1}/(k D_h^{n-1})$
$\ddot{q}_w$	wall heat flux [W m^{-2}]
Re	Reynolds number, $Re = \rho U_0^{2-n} D_h^n / m$
T	temperature [K]
T_0	inlet temperature [K]
U_0	inlet velocity [m s^{-1}]
U_{max}	velocity at $y = 0$ in the hydrodynamically developed region [m s^{-1}]

$U(x)$	velocity in the core region of the developing flow [m s^{-1}]
u, v	velocity components [m s^{-1}]
x, y	Cartesian coordinates [m]
x^*	non-dimensional axial position $x^* = x/(D_h Re)$
$\hat{x}$	non-dimensional axial position $\hat{x} = x/(D_h Re Pr)$
z	non-dimensional boundary layer thickness $z = \delta/b$

Greek letters

Δ, Δ_{th}	thickness of core region for hydrodynamic, thermal problems [m]
δ, δ_{th}	boundary layer thickness for hydrodynamic, thermal problems [m]
ϵ	$= (n+1)/n$
θ	non-dimensional temperature, $\theta = (T - T_0)/(\ddot{q}_w b/k)$
ρ	density [kg m^{-3}]
σ	stress [Pa]

Subscripts

b	bulk
fd	fully developed

hydrodynamic entry problem for the pseudo-Newtonian flow and obtained a single correlation (independent of the flow behavior index) between the pressure drop and the axial distance which agrees well, for $Re > 500$, with experimental data from the literature. Cotta and Özişik [9] used the sign-count method to solve the thermal entrance region heat transfer for laminar forced convection of power-law fluids inside a circular tube and parallel plate channel with the T condition. They presented the local Nusselt number for the entrance region for fluids with values of the flow behavior index $n = 1/3; 1; 3$. Magno et al. [10,11] used the generalized integral transform technique to solve numerically the boundary layer equations for simultaneously developing laminar flow of power-law fluids in a parallel plates channel with the T condition as well. They presented the bulk temperature and Nusselt number at different axial positions along the channel for various flow behavior indices and apparent Prandtl numbers. They noted that for flow behavior indices greater than unity the convective effects near the wall diminish and result in lower values for the Nusselt number in the entrance region. In the thermally developed region they found that, for a fixed value of the apparent Prandtl number, the Nusselt number is essentially independent of the flow behavior index. Gupta [12] applied he transformation method by Matras & Nowak [8] to hydrodynamically developing isothermal flows of power-law fluids in circular pipes and parallel-plates ducts and compared the results of four integral approaches used to solve the equivalent pseudo-Newtonian flow. Recently, Galanis & Rashidi [13] obtained a new solution for the Graetz problem extended to power-law fluids and mass transfer with phase change at the walls. The temperature and concentration spatial distributions were used to illustrate the effects of the fluid nature on the axial evolution of the sensible and latent Nusselt numbers as well as on the local entropy generation due to velocity, temperature and concentration gradients.

Our literature search has yielded few studies for forced convection of power-law fluids in ducts with the H condition (constant uniform heat flux). Cotta & Özişik [14] addressed this problem for hydrodynamically developed flows in circular tubes and

parallel-plate ducts and derived exact expressions for the local and average Nusselt numbers. However, to the best of our knowledge, the simultaneously developing hydrodynamic and thermal flow of power-law fluids in ducts with the H condition has not been treated. In view of this situation the present study was undertaken. It presents approximate analytical expressions for the velocity and temperature distributions in the entrance region of the duct which match the corresponding exact expressions at L_{hy} and L_{th} respectively. These expressions are used to calculate the axial evolution of the friction coefficient and the Nusselt number for different fluids.

2. Statement of the problem

We consider the two-dimensional flow of an incompressible power-law fluid with constant properties between two parallel plates (Fig. 1). A constant uniform heat flux is applied at the two solid-fluid interfaces. At the duct inlet ($x = 0$) the velocity and temperature of the fluid are constant and uniform (respectively U_0 and T_0 with the former parallel to the plates). Therefore this is a steady-state forced convection problem, i.e. the hydrodynamic field does not depend on the temperature. In Fig. 1 δ and δ_{th} are the
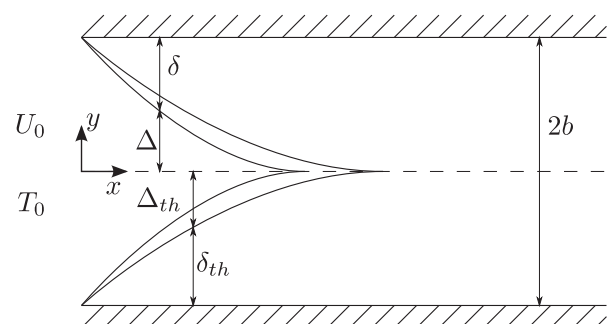

Fig. 1. Schematic configuration of the problem under study.

hydrodynamic and thermal boundary layer thicknesses respectively; Δ and Δ_{th} are the distances between the edge of these two boundary layers and the symmetry plane at $y = 0$.

3. Solution of the hydrodynamic field

3.1. Hydrodynamically developed region

The equations of continuity and motion in the hydrodynamically developed region ($x > L_{hy}$) where $v = 0$ are

$$\rho \left(\frac{\partial u}{\partial x} \right) = 0 \tag{1}$$

$$\frac{\partial P}{\partial x} + \frac{\partial \sigma_{yx}}{\partial y} = 0 \tag{2}$$

$$\left(\frac{\partial P}{\partial y} \right) = 0 \tag{3}$$

For a power-law fluid

$$\sigma_{yx} = m \left(\frac{\partial u}{\partial y} \right)^n \tag{4}$$

Therefore u does not depend on x, P does not depend on y and $\partial P / \partial x$ is equal to a constant. By replacing Eq. (4) in Eq. (2), integrating the resulting expression with respect to y and taking into account the no-slip condition ($u = 0$ at $y = b$) we obtain the following expression for the velocity profile in the hydrodynamically developed region

$$u(x \geqslant L_{hy}, y) = \left(\frac{1}{m} \frac{dP}{dx} \right)^{1/n} \left(\frac{n}{n+1} \right) (b^\epsilon - y^\epsilon) \tag{5a}$$

The velocity profile is symmetrical with respect to the plane $y = 0$ where it reaches its maximum value. Finally by applying the integral form of mass conservation between $x = 0$ and $x = L_{hy}$ we obtain the following two relations:

$$\frac{u(x \geqslant L_{hy}, y)}{U_{max}} = 1 - \left(\frac{y}{b} \right)^\epsilon \tag{5b}$$

$$\frac{U_{max}}{U_0} = \frac{2n+1}{n+1} \tag{5c}$$

These relations are identical to those obtained by Yau & Tien [6]. For a Newtonian fluid ($n = 1$) they reduce to the well known results for plane Poiseuille flow.

3.2. Hydrodynamically developing region

Following previous studies [6,15] it is assumed that in the developing region ($L_{hy} \geqslant x \geqslant 0$) the flow field consists of a boundary layer of thickness $\delta(x)$ and a core of thickness $\Delta = b - \delta$. Extending the approach adopted by Campbell & Slattery [15] who restricted their analysis to Newtonian fluids we assume that the velocity is

$$u(x, y) = U(x), \quad \text{for} \quad \Delta \geqslant y \geqslant 0 \tag{6a}$$

and

$$\frac{u(x, y)}{U(x)} = 1 - \left(\frac{y - \Delta}{b - \Delta} \right)^\epsilon, \quad \text{for} \quad b \geqslant y \geqslant \Delta \tag{6b}$$

These expressions satisfy the matching condition at $y = \Delta$.

In order to evaluate the core velocity $U(x)$ and the boundary layer thickness $\delta(x)$, or its complement $\Delta(x)$, we apply the integral forms of the continuity and momentum equations between the

duct inlet ($x = 0$) and an arbitrary position in the entrance region ($0 < x \leqslant L_{hy}$) and thus obtain the following two relations:

$$\frac{U(x)}{U_0} \left[1 - \frac{n}{2n+1} \left(1 - \frac{\Delta}{b} \right) \right] = 1 \tag{7}$$

$$\frac{P_0 - P(x)}{\frac{1}{2}\rho U_0^2} - \left(\frac{n+1}{n} \right)^n \frac{2m[U(x)]^{n-2}}{b^n \rho (1 - \frac{\Delta}{b})^n} \left(\frac{U(x)}{U_0} \right)^2 \frac{x}{b}$$
$$= 2 \frac{\Delta}{b} \left(\frac{U(x)}{U_0} \right)^2 + \frac{4(n+1)^2}{(3n+2)(2n+1)} \left(1 - \frac{\Delta}{b} \right) \left(\frac{U(x)}{U_0} \right)^2 - 2 \tag{8}$$

At the duct inlet ($x = 0$) where $\Delta = b$ (or, equivalently, $\delta = 0$) Eq. (7) reduces to $U(x) = U_0$ and thus satisfies the inlet condition. Furthermore, at $x = L_{hy}$ where $\Delta = 0$ (or, equivalently, $\delta = b$) it gives $U(x) = (2n+1)/(n+1) = U_{max}$ and Eq. (6b) becomes identical to Eq. (5b) for all values of the flow behavior index. Thus the assumed profile is more appropriate than the 4th order polynomial used by Yau & Tien [6] which reduces to the exact analytical profile at $x = L_{hy}$ only for three particular values of the flow behavior index ($n = 1, 1/2$ and $1/3$).

Eqs. (7) and (8) relate the two unknown functions $U(x)$ and $\Delta(x)$ but also include the non-dimensional pressure drop between the two sections under consideration. A third equation is therefore required to close the system and this is obtained by applying the differential equation of motion in the x-direction at the symmetry axis ($y = 0$). Because of symmetry the transversal velocity component at $y = 0$ is zero. Furthermore in the core the velocity is independent of y. Therefore at $y = 0$ the stress tensor is identically zero. Integration of this simplified form of the equation of motion between the two sections under consideration leads to the Bernoulli relation for frictionless flow. When Eqs. (6a), (6b) for the velocity profile are replaced in the Bernoulli relation we obtain the following:

$$\frac{P_0 - P(x)}{\frac{1}{2}\rho U_0^2} = \left(\frac{U(x)}{U_0} \right)^2 - 1 \tag{9}$$

It should be noted that as reported by Campbell & Slattery [15] the Bernoulli equation was similarly used by Schiller who studied the entry hydrodynamic problem for Newtonian fluids.

By combining Eqs. (7)–(9) we obtain the following explicit relation between the non-dimensional axial position and the non-dimensional boundary layer thickness:

$$x^* = 2^{-2n-3} \left(\frac{n}{(n+1)} \right)^n z^{n+1} \left[1 - \frac{n}{2n+1} z \right]^{n-2}$$
$$\times \left[\frac{2n(n+1)}{(3n+2)(2n+1)} + \left(\frac{n}{2n+1} \right)^2 z \right] \tag{10}$$

For any given value of the flow behavior index it is therefore possible to choose a value of the non-dimensional boundary layer thickness and to calculate the corresponding axial position from Eq. (10), the corresponding core velocity from Eq. (7) and the corresponding pressure loss from Eq. (9). In particular, by setting $z = 1$ (i.e. $\delta = b$) we obtain the following expression for the non-dimensional hydrodynamic development length:

$$L_{hy}^* = \frac{n^{n+1}(7n^2 + 8n + 2)}{2^{2n+3}(n+1)^2(3n+2)(2n+1)^n} \tag{11}$$

Furthermore, since the velocity profile in both the developing and hydrodynamically developed regions is known (see Eqs. (5b) and (5c), and Eqs. (6a) and (6b) respectively) it is possible to calculate the corresponding wall shear stress and the skin friction coefficient from

$$C_f Re = \left(\frac{2\sigma_w}{\rho U_0^2}\right) Re = \frac{2D_h{}^n |du/dy|^n}{U_0^n} \tag{12a}$$

Thus, in the hydrodynamically developed region

$$C_f Re = 2\left(\frac{2n+1}{n}\right)^n \left(\frac{D_h}{b}\right)^n \tag{12b}$$

and in the developing region

$$C_f Re = \left(\frac{n+1}{n}\right)^n \frac{2^{2n+1}}{(\delta/b)^n \left[1 - \frac{n}{2n+1}(\delta/b)\right]^n} \tag{12c}$$

3.3. Results for the hydrodynamic field

Figs. 2 and 3 compare the predictions of the present approximate analytical solution for $n = 1$ (Newtonian fluid) with the numerical results by Bodoia & Osterle [1] which are the most precise according to Shah & Bhati [4]. Fig. 2 shows the velocity profiles at three axial positions while Fig. 3 shows the axial evolution of the velocity for three transversal positions. In all cases the agreement between the present and previous results is very good (the differences for all x^* are smaller than 4% at $y = 0$ and less than 10% at $y/b = 0.9$) and improves as the distance from the inlet increases (at $x^* = 0.125$ the differences for all y are less than 1%). The skin friction coefficient for $n = 1$ at $x^* = L_{hy}^*$ can be calculated from Eq. (12b) or (12c) (by setting $\delta = b$) and is

$$C_f Re = 24 \tag{13}$$

This value is identical to the exact analytical result. These preliminary comparisons indicate that the present model gives satisfactory results for the hydrodynamic field of Newtonian fluids.

For non-Newtonian fluids the present expression for the fully developed velocity profile (Eqs. (5b) and (5c)) is identical to that given elsewhere [6,13,16]. Comparisons of other important predictions of the present solution for $n \neq 1$ with the corresponding results calculated by Yau & Tien [6] and by Magno et al. [10] are presented and discussed in the following paragraphs.

Fig. 4 shows the effect of the flow behavior index on the non-dimensional hydrodynamic development length and compares the present results from Eq. (11) with other published data. Qualitatively the present predictions agree with those by Yau & Tien [6].
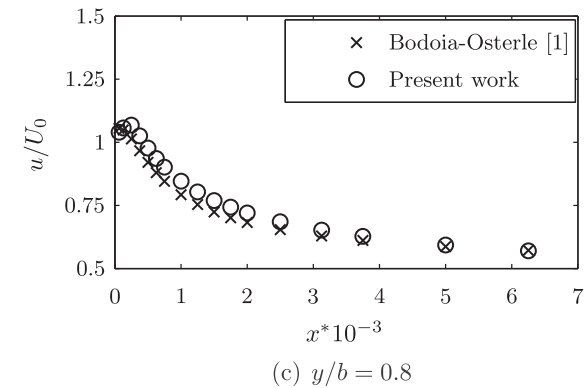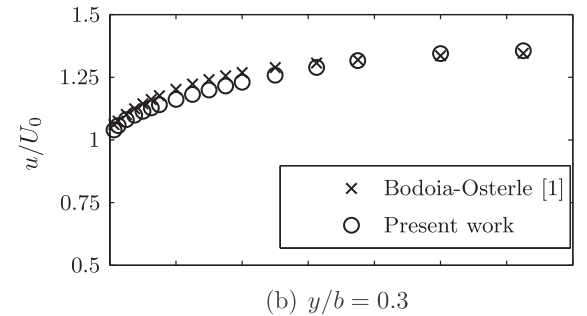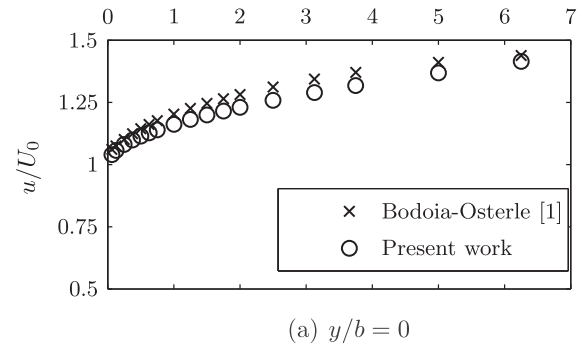
Fig. 3. Evolution of the axial velocity component for Newtonian fluid at three transversal positions.
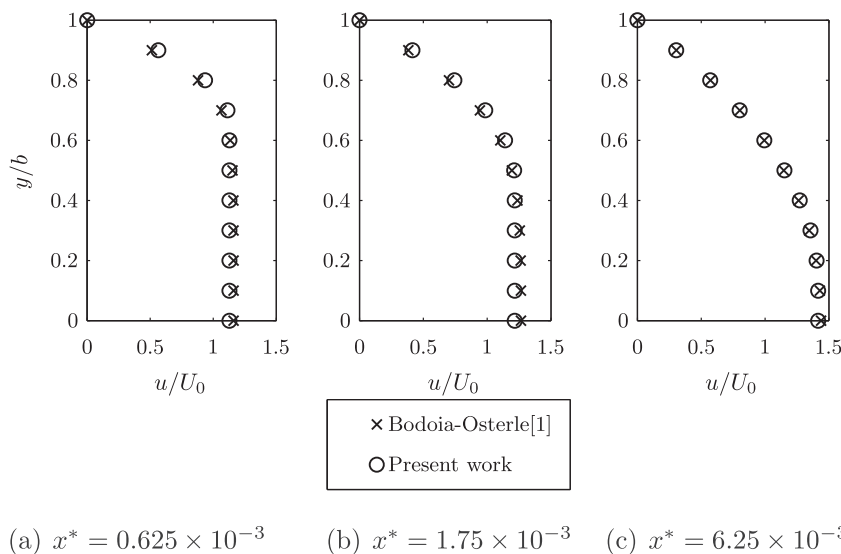
(a) $x^* = 0.625 \times 10^{-3}$ (b) $x^* = 1.75 \times 10^{-3}$ (c) $x^* = 6.25 \times 10^{-3}$

Fig. 2. Velocity profiles for Newtonian fluid at different axial positions.
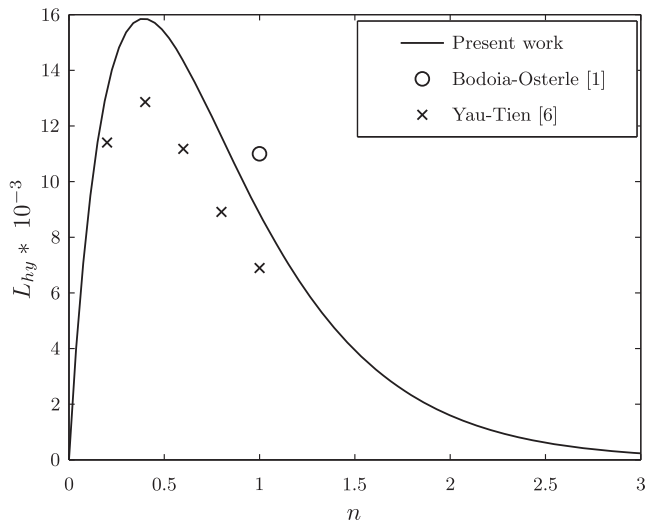
Fig. 4. Hydrodynamic entrance length versus the flow behavior index.

(a) $n = 0.75$

(b) $n = 1$

(c) $n = 3$

Fig. 5. Evolution of the centerline axial velocity component.

Fig. 6. Evolution of the non-dimensional hydrodynamic boundary layer thickness.

They both indicate that L_{hy} is maximum for $n = 0.4$. However, the values predicted by these two models differ considerably. Since the present result for Newtonian fluids is closer to the value calculated by Bodoia & Osterle [1] the present model is deemed to be more accurate than the one by Yau & Tien [6]. It should be noted that the values of L_{hy} calculated by Magno et al. [10] are much higher than those presented in Fig. 4. Thus, for example, their value for $n = 0.75$ is approximately 23 times higher than the corresponding one by Yau & Tien [6].

Fig. 5 presents the evolution of the axial velocity component at the symmetry axis ($y = 0$) for three values of the flow behavior index and compares the present results with corresponding published data. Qualitatively the agreement is always good. It is noted however that the predictions by Yau & Tien [6] as well as those by Magno et al. [10] are always higher than those of the present model. For Newtonian fluids ($n = 1$) the values predicted by Magno et al. [10] are in better agreement with those calculated by Bodoia & Osterle [1]. However the present predictions are always within 4.1% of those by Bodoia & Osterle [1].

Fig. 6 shows the evolution of the non-dimensional boundary layer thickness for three values of the flow behavior index. The present results for $n = 0.5$ are quite similar to those obtained by Yau & Tien [6] although their results indicate a thicker boundary layer and a shorter hydrodynamic development length (see also Fig. 4). It is interesting to note that the boundary layer thickness at any given axial position does not vary monotonically with the flow behavior index. It is thinnest for $n = 0.5$ and thickest for $n = 3$.

Finally, Fig. 7 shows the evolution of the dimensionless pressure drop for three values of the flow behavior index. Qualitatively the predictions of the present model agree with previously published results and confirm the fact that the pressure drop increases with the flow behavior index [6]. However the present results for $n = 1$ (Newtonian fluid) underestimate the numerical predictions of Bodoia & Osterle [1] by almost 20%. This is due to the simplifications associated with the application of the Bernoulli equation (see discussion by Campbell & Slattery [15]) who used an integral form of the energy equation instead of the Bernoulli equation in their study of isothermal flow of a Newtonian fluid in the entrance region of a circular duct; in the present case the integral form of the energy equation is used for the calculation of the thermal field, see Section 4b). Despite this problem we believe that the explicit analytical expressions of the present model constitute a valid tool for preliminary calculations of non-Newtonian flow characteristics.
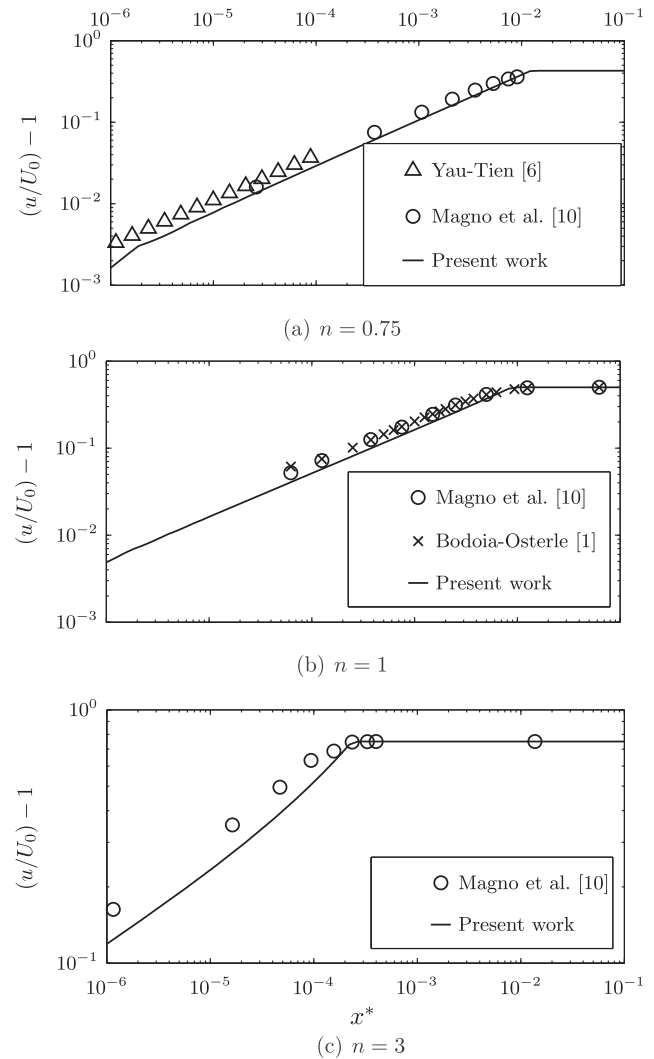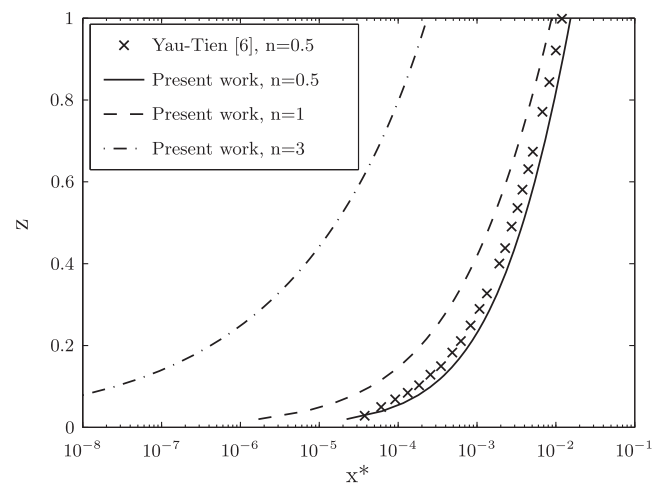
4. Solution of the thermal field

As in previous studies [1,5,6,11,13] it is assumed that longitudinal conduction of heat and the effects of viscous dissipation are
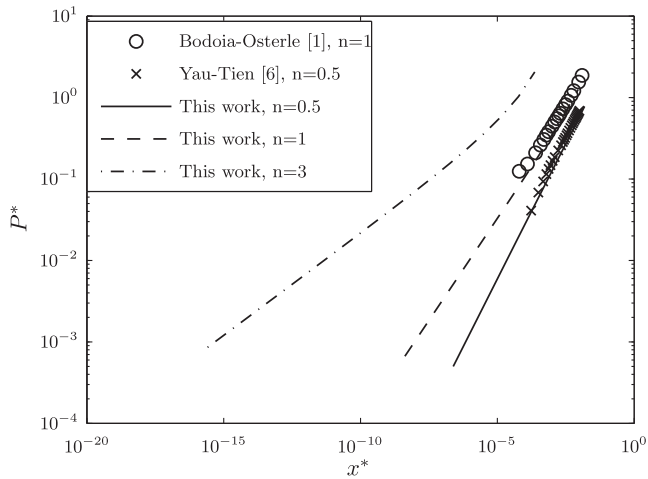
Fig. 7. Evolution of the non-dimensional pressure drop.

negligible. Hence, the energy equation in the fully developed region is

$$k\frac{\partial^2 T}{\partial y^2} = \rho u_{fd} c_p A \tag{14a}$$

where, for the H condition

$$A = \left|\frac{\partial T}{\partial x}\right|_{fd} = \left|\frac{dT_w}{dx}\right|_{fd} = \left|\frac{dT_b}{dx}\right|_{fd} \tag{14b}$$

and

$$\frac{dT_b}{dx} = \frac{2\ddot{q}_w}{\dot{m}c_p} = \frac{\ddot{q}_w}{\rho c_p U_0 b} \tag{14c}$$

Therefore the energy equation in the fully developed region becomes

$$k\frac{\partial^2 T}{\partial y^2} = \frac{u_{fd}\ddot{q}_w}{bU_0} \tag{14d}$$

Integration of Eq. (14c) and application of the condition at the inlet where $T_b = T_0$ gives the following expression for the bulk temperature

$$T_b = T_0 + \frac{\ddot{q}_w x}{\rho c_p U_0 b} \tag{15a}$$
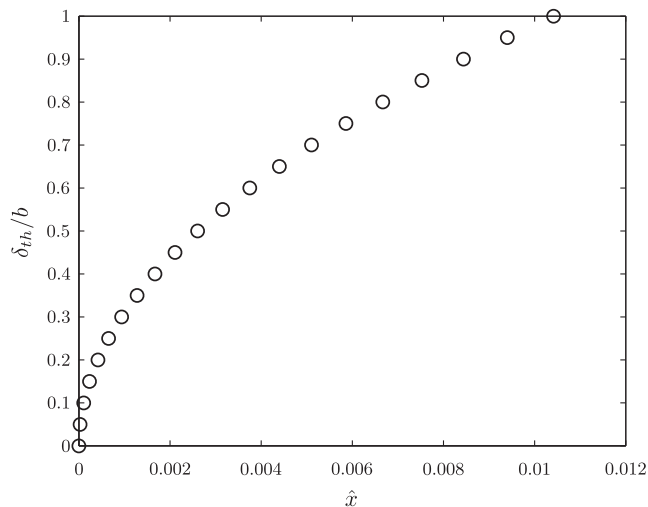

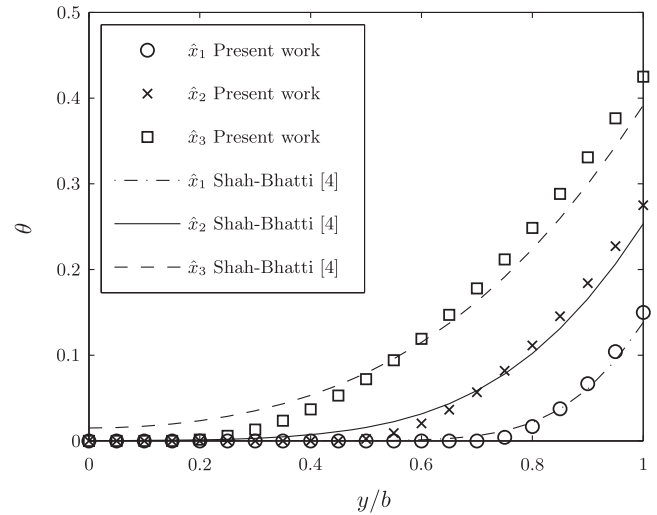Fig. 8. Evolution of the thermal boundary thickness for slug flow.

Fig. 9. Temperature profiles at three axial positions ($\hat{x}_1 = 0.938 \times 10^{-3}$, $\hat{x}_2 = 3.151 \times 10^{-3}$, $\hat{x}_3 = 7.526 \times 10^{-3}$) in the thermally developing region for slug flow.
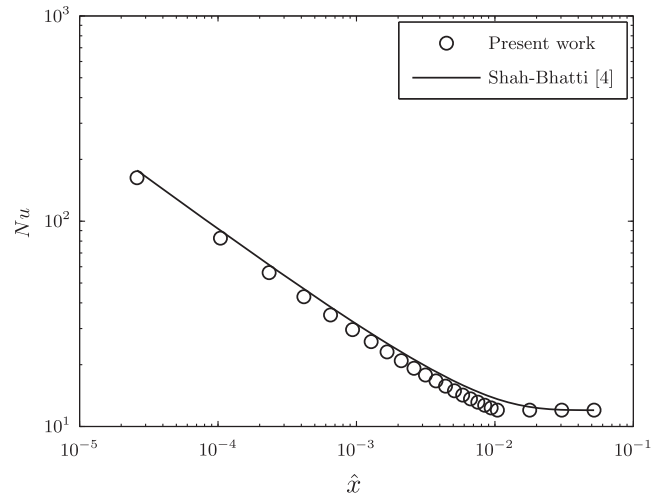

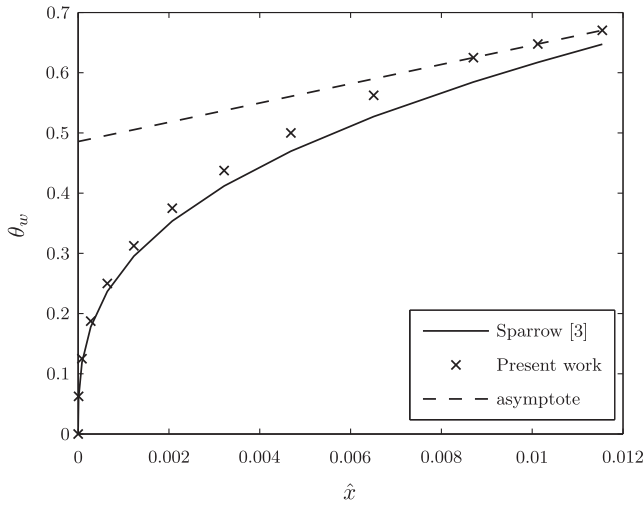Fig. 10. Evolution of the Nusselt number for slug flow.

or in non-dimensional form

$$\theta_b = 16\hat{x} \tag{15b}$$

In the thermally developing region we assume, analogously to the treatment in Section 3, that the temperature depends on the distance from the centerline within the boundary layer but is uniform in the core region ($|y| \leqslant \Delta_{th}$). In fact, in order to ensure that this profile matches the imposed value of the inlet temperature, the fluid temperature within the thermal core region is everywhere equal to T_0. At the centerline in particular the fluid temperature remains equal to T_0 up to $x = L_{th}$ and then increases linearly as indicated by the combination of Eqs. (14b) and (14c).

In the following three subsections the solution of Eq. (14d) as well as the temperature distribution in the thermally developing region is presented for the following three particular cases since we were not able to obtain a general solution:

- slug flow for which $u_{fd} = U_0$ (i.e. $L_{hy} \gg L_{th}$),
- hydrodynamically developed flow for which u_{fd} is given by Eq. (5) (i.e. $L_{hy} \ll L_{th}$) and

Fig. 11. Evolution of the wall temperature in the thermal entrance region for hydrodynamically developed flow of a Newtonian fluid.

Fig. 13. Evolution of the boundary layer thickness for hydrodynamically developed flow.
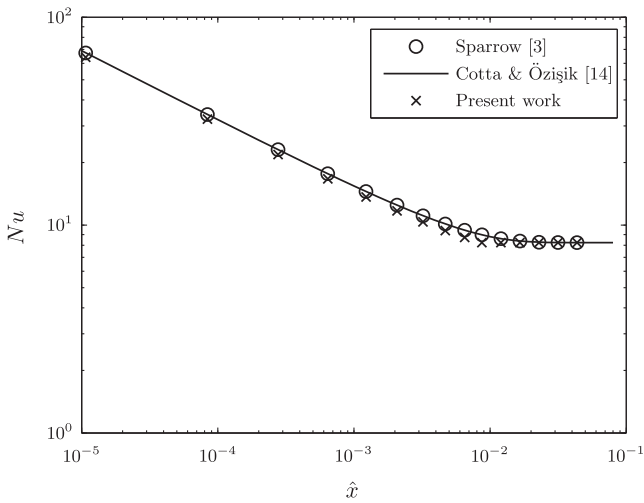
Fig. 12. Evolution of the Nusselt number in the thermal entrance region for hydrodynamically developed flow of a Newtonian fluid.

- flows with identical hydrodynamic and thermal boundary layer thicknesses ($\delta = \delta_{th}$).

It should be noted that not all the results presented in the previous section on the hydrodynamic problem are used in the solution of these thermal problems due to the simplifying assumptions inherent in each of these cases.

As mentioned before, the thermal entrance problem for flow between parallel plates with the H condition has not been treated in the literature. Therefore comparisons of the proposed solutions with previously published results are only given for the case of Newtonian fluids ($n = 1$) and for the case of hydrodynamically developed flow for which such results are available.

4.1. Slug flow

As pointed out by Shah & Bhatti [4] when the Prandtl number is smaller than unity the temperature profile develops faster than the velocity profile. In the limiting case with $Pr = 0$ the velocity profile remains constant (slug flow) while the temperature profile
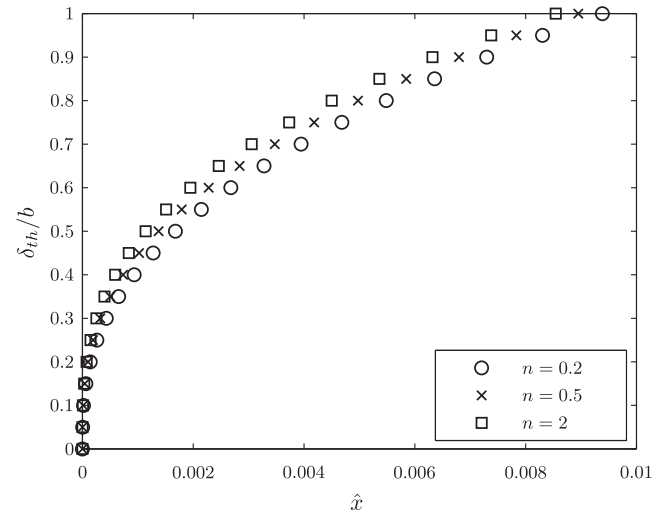
develops. In this case none of the results of Section 3 regarding the hydrodynamic field are used since $u_{fd} = U_0$. With this condition the energy equation in the developed region (Eq. (14d)) becomes

$$k\left(\frac{\partial^2 T}{\partial y^2}\right) = \frac{\ddot{q}_w}{b} \tag{16a}$$

This can be readily integrated and by applying the boundary condition at $y = b$ where $k(\partial T/\partial y) = \ddot{q}_w$ as well as the expression for $\partial T/x$ resulting from the combination of Eqs. (14b) and (14c) we obtain

$$kT(x \geqslant L_{th}, y) = \frac{\ddot{q}_w b}{2}\left(\frac{y}{b}\right)^2 + \frac{k\ddot{q}_w}{\rho c_p u_0 b}x + C \tag{16b}$$

The value of C is obtained by applying Eq. (16b) at $(x = L_{th}, y = 0)$ where, according to the argument in the paragraph following Eq. (14d), the fluid temperature is equal to T_0. Thus

$$T(x \geqslant L_{th}, y) = T_0 + \left(\frac{\ddot{q}_w b}{2k}\right)\left(\frac{y}{b}\right)^2 + \frac{\ddot{q}_w(x - L_{th})}{\rho c_p U_0 b} \tag{16c}$$

or in non-dimensional form

$$\theta(\hat{x}, y) = \frac{1}{2}\left(\frac{y}{b}\right)^2 + 16(\hat{x} - \widehat{L}_{th}) \tag{16d}$$

In order to obtain the expression for the temperature distribution in the developing region we assume, analogously to the treatment of the hydrodynamic problem, that in the y-direction its distribution in the thermal boundary layer is similar to that in the developed region. Thus, the expression for the fluid temperature in the developing region is

$$T(x, y) = T_0 \text{ or, equivalently, } \theta(\hat{x}, y) = 0 \quad \text{for } 0 \leqslant y \leqslant \Delta_{th} \tag{17a}$$

$$\theta(\hat{x}, y) = \frac{1}{2}\left(\frac{y - \Delta_{th}}{b - \Delta_{th}}\right)^2\left(1 - \frac{\Delta_{th}}{b}\right) \quad \text{for } \Delta_{th} \leqslant y \leqslant b \tag{17b}$$

This formulation satisfies all the conditions at $(0 \leqslant x \leqslant L_{th}, y = \Delta_{th})$ and becomes identical to the corresponding expression for the developed region (Eq. (16d)) at $x = L_{th}$ where $\Delta_{th} = 0$.

The thermal entrance length can be obtained by applying the integral form of the energy equation between $x = 0$ and $x = L_{th}$

$$2L_{th}\ddot{q}_w = 2\rho c_p \int_0^b u[T(x = L_{th}, y)T_0]dy \tag{18a}$$

When the expression for the temperature, Eq. (16c), is replaced and the integral is evaluated we obtain the following result for the case under consideration

$$\frac{L_{th}}{D_h} = \frac{RePr}{96} \approx 0.0104 RePr \tag{18b}$$

This result differs by less than 10% from the corresponding one for thermally developing flow of Newtonian fluids [4].

Finally, in order to obtain a relation between the thermal boundary layer thickness and the axial position we apply the integral form of the energy equation between $x = 0$ and $x < L_{th}$

$$2x\ddot{q}_w = 2\rho c_p \int_0^b u[T(x,y)T_0]dy \tag{19a}$$

When the expression for the temperature, Eq. (17), is replaced and the integral is evaluated we obtain the following result for the case under consideration

$$\hat{x} = \frac{(\delta_{th}/b)^2}{96} \tag{19b}$$

This expression for the axial variation of the thermal boundary layer is compatible with Eq. (15b) (since Eq. (19a) is the same as Eq. (14c)) and with Eq. (18b) (since $\delta_{th} = b$ at $x = L_{th}$).

It is interesting to note that with this standard non-dimensional formulation the temperature profile as well as the thermal entrance length and the boundary layer thickness are all independent of the flow behavior index for the case of slug flow. Fig. 8 shows the relation between δ_{th}/b and $\hat{x}$, Fig. 9 shows the non-dimensional temperature profile at different axial positions and Fig. 10 shows the axial evolution of the Nusselt number for the particular case under consideration. The latter was obtained from the following relation

$$Nu = \frac{\ddot{q}_w D_h}{k(T_w T_b)} = \frac{4}{\theta_w - \theta_b} \tag{20}$$

where the wall temperature is obtained by setting $y = b$ in Eq. (17b) and the bulk temperature is given by Eq. (15). Figs. 9 and 10 show that the present predictions are in good agreement with corresponding results quoted by Shah & Bhatti [4, section 3.3.4] for a Newtonian fluid with $Pr = 0$. In particular, according to the present solution for slug flow the value of the Nusselt number in the thermally developed region is 12, i.e. identical to the corresponding value in the literature [4, p. 3–44]. On the other hand, the thermal entrance length predicted by Eq. (18b) is only 65% of the corresponding value for a Newtonian fluid with $Pr = 0$.
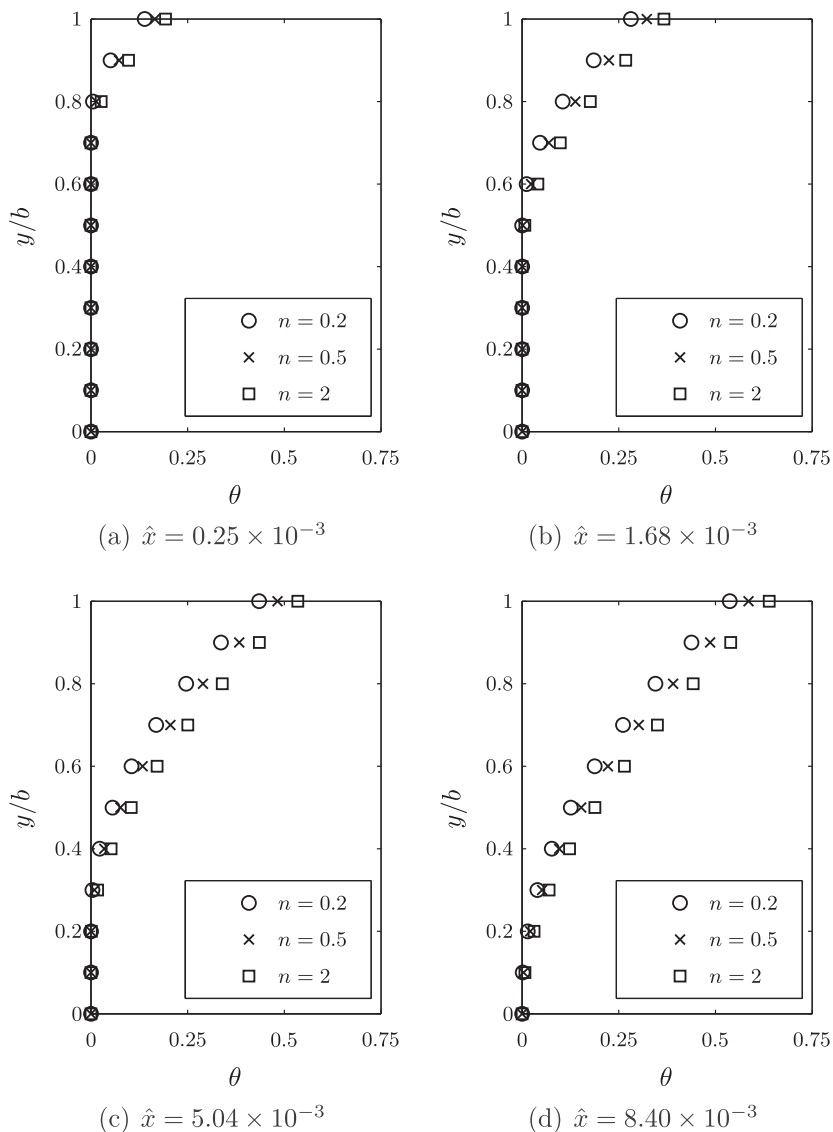

(a) $\hat{x} = 0.25 \times 10^{-3}$

(b) $\hat{x} = 1.68 \times 10^{-3}$

(c) $\hat{x} = 5.04 \times 10^{-3}$

(d) $\hat{x} = 8.40 \times 10^{-3}$

Fig. 14. Non-dimensional temperature profiles at four axial positions for hydrodynamically developed flow.

4.2. Hydrodynamically developed flow

As pointed out by Shah & Bhatti [4] this assumption is reasonable for fluids with high Prandtl numbers for which the velocity profile develops much more rapidly than the temperature profile. In the limiting case with $Pr = \infty$ it is then acceptable to consider that the velocity profile throughout the flow field is given by Eq. (5). Therefore the energy equation in the thermally developed region (Eq. (14d)) becomes

$$k\frac{\partial^2 T}{\partial y^2} = \frac{2n+1}{n+1}\left[1 - \left(\frac{y}{b}\right)^{\frac{n+1}{n}}\right]\frac{q_w''}{b} \tag{21a}$$

This is integrated and after applying the boundary condition at $y = b$ where $k(\partial T/\partial y) = \ddot{q}_w$ as well as the condition resulting from Eq. (14b) we obtain the following expression

$$kT(x \geqslant L_{th}, y) = \ddot{q}_w b\frac{2n+1}{2(n+1)}\left(\frac{y}{b}\right)^2 - \ddot{q}_w b\frac{n^2}{(n+1)(3n+1)}\left(\frac{y}{b}\right)^{\frac{3n+1}{n}} + \frac{k\ddot{q}_w}{\rho c_p U_0 b}x + C \tag{21b}$$

The value of the constant C is evaluated by noting that $T(x = L_{th}, 0)$ is equal to T_0. Therefore

$$T(x \geqslant L_{th}, y) = T_0 + \frac{\ddot{q}_w b(2n+1)}{2k(n+1)}\left(\frac{y}{b}\right)^2 - \frac{\ddot{q}_w b n^2}{k(n+1)(3n+1)}\left(\frac{y}{b}\right)^{\frac{3n+1}{n}} + \frac{\ddot{q}_w(x - L_{th})}{\rho c_p U_0 b} \tag{21c}$$

The corresponding non-dimensional expression is

$$\theta(\hat{x} \geqslant \widehat{L}_{th}, y) = \frac{2n+1}{2(n+1)}\left(\frac{y}{b}\right)^2 - \frac{n^2}{(n+1)(3n+1)}\left(\frac{y}{b}\right)^{\frac{3n+1}{n}} + 16(\hat{x} - \widehat{L}_{th}) \tag{21d}$$

The corresponding temperature profile in the thermally developing region is again obtained by assuming that in the y-direction its distribution in the thermal boundary layer is similar to that in the developed region. Thus, the expression for the fluid temperature in the developing region is

$$T(x, y) = T_0 \text{ or, equivalently, } \theta(\hat{x}, y) = 0 \quad \text{for } 0 \leqslant y \leqslant \Delta_{th} \tag{22a}$$

$$\theta(\hat{x}, y) = \left(1 - \frac{\Delta_{th}}{b}\right)\frac{1}{n+1} \times \left[\frac{2n+1}{2}\left(\frac{y - \Delta_{th}}{b - \Delta_{th}}\right)^2 - \frac{n^2}{(3n+1)}\left(\frac{y - \Delta_{th}}{b - \Delta_{th}}\right)^{\frac{3n+1}{n}}\right] \tag{22b}$$

The thermal entrance length is again obtained by applying the integral form of the energy equation between $x = 0$ and $x = L_{th}$ (Eq. (18a)). The integral on the right hand side of this equation is in this case more complicated since both the velocity and temperature depend on the y-coordinate. The result of the lengthy operations which are not presented here is

$$\widehat{L}_{th} = \frac{(2n+1)(24n^2 + 13n + 2)}{96(3n+1)(4n+1)(5n+2)} \tag{23}$$

As before, in order to obtain the relation between the thickness of the thermal boundary layer and the axial position we apply the energy equation between $x = 0$ and $x < L_{th}$ (Eq. (19a)). The result of the corresponding lengthy operations is
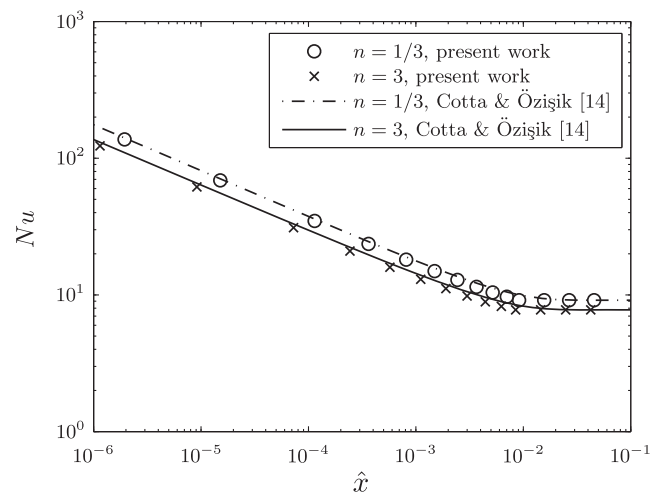
$$\hat{x} = \frac{2n+1}{16(n+1)}\left(\frac{\delta_{th}}{b}\right)I' = \frac{2n+1}{16(n+1)}\left(\frac{\delta_{th}}{b}\right)[I_A' - (I_{B1}' + I_{B2}')] \tag{24}$$
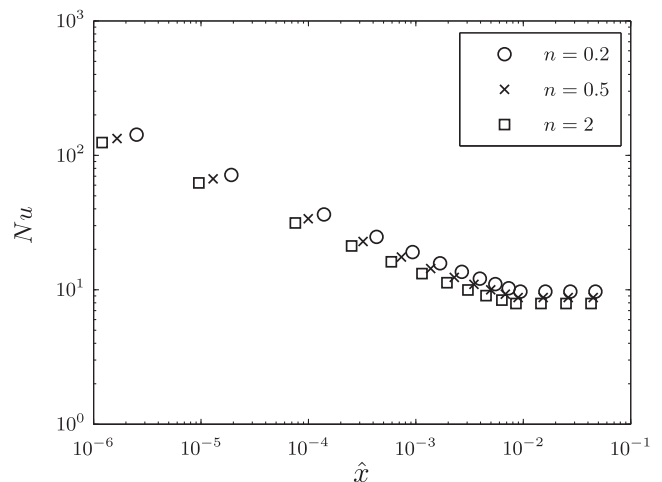
where

$$I_A' = \int_0^b \frac{2n+1}{2(n+1)}\left(\frac{y - \Delta_{th}}{b - \Delta_{th}}\right)^2 dy - \int_0^b \times \frac{n^2}{(n+1)(3n+1)}\left(\frac{y - \Delta_{th}}{b - \Delta_{th}}\right)^{\frac{3n+1}{n}} dy = \left(1 - \frac{\Delta_{th}}{b}\right)\left[\frac{2n+1}{6(n+1)} - \frac{n^3}{(n+1)(3n+1)(4n+1)}\right] \tag{25a}$$

$$I_{B1}' = \frac{2n+1}{2(n+1)}\int_{\Delta_{th}}^b \left(\frac{y}{b}\right)^{\frac{n+1}{n}}\left(\frac{y - \Delta_{th}}{b - \Delta_{th}}\right)^2 dy = \frac{2n+1}{2(n+1)}\left(1 - \frac{\Delta_{th}}{b}\right)^{-2}\left[\frac{n}{4n+1} - \frac{2n}{3n+1}\frac{\Delta_{th}}{b} + \frac{n}{2n+1}\left(\frac{\Delta_{th}}{b}\right)^2 - \frac{2n^3}{(2n+1)(3n+1)(4n+1)}\left(\frac{\Delta_{th}}{b}\right)^{\frac{4n+1}{n}}\right] \tag{25b}$$

$$I_{B2}' = \int_{\Delta_{th}}^b \frac{n^2(y/b)^{\frac{n+1}{n}}}{(n+1)(3n+1)}\left(\frac{y - \Delta_{th}}{b - \Delta_{th}}\right)^{\frac{3n+1}{n}} dy \tag{25c}$$

(a) Validation

(b) Present work results

Fig. 15. Evolution of the Nusselt number for hydrodynamically developed flow.
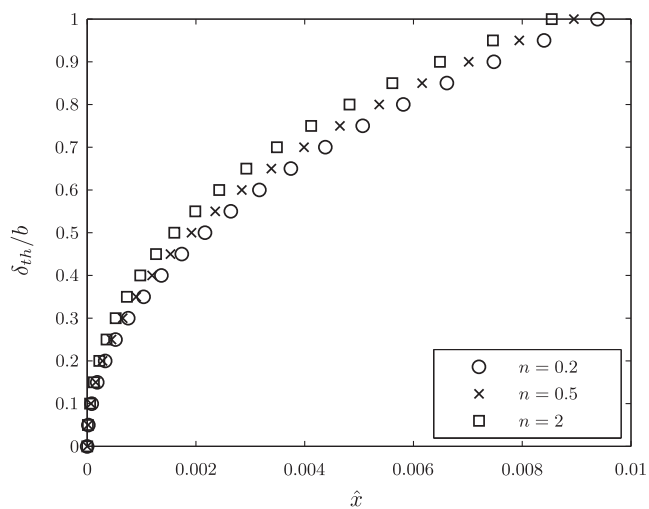
Fig. 16. Evolution of the thermal boundary thickness for $\delta = \delta_{th}$.
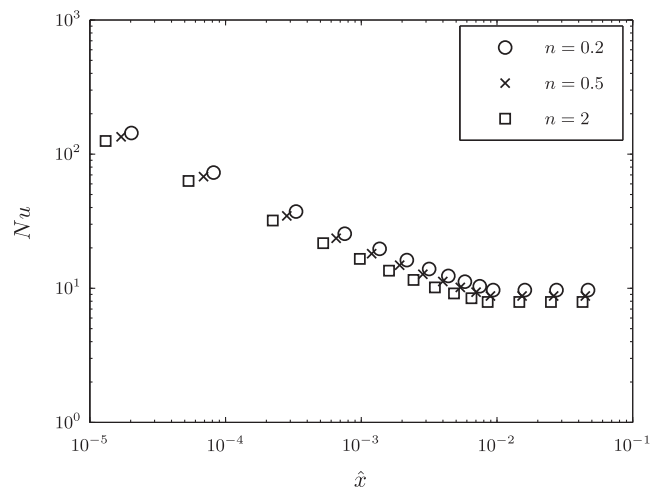

Fig. 18. Evolution of the Nusselt number for $\delta = \delta_{th}$.

(a) $\hat{x} = 0.25 \times 10^{-3}$

(b) $\hat{x} = 1.68 \times 10^{-3}$

(c) $\hat{x} = 5.04 \times 10^{-3}$
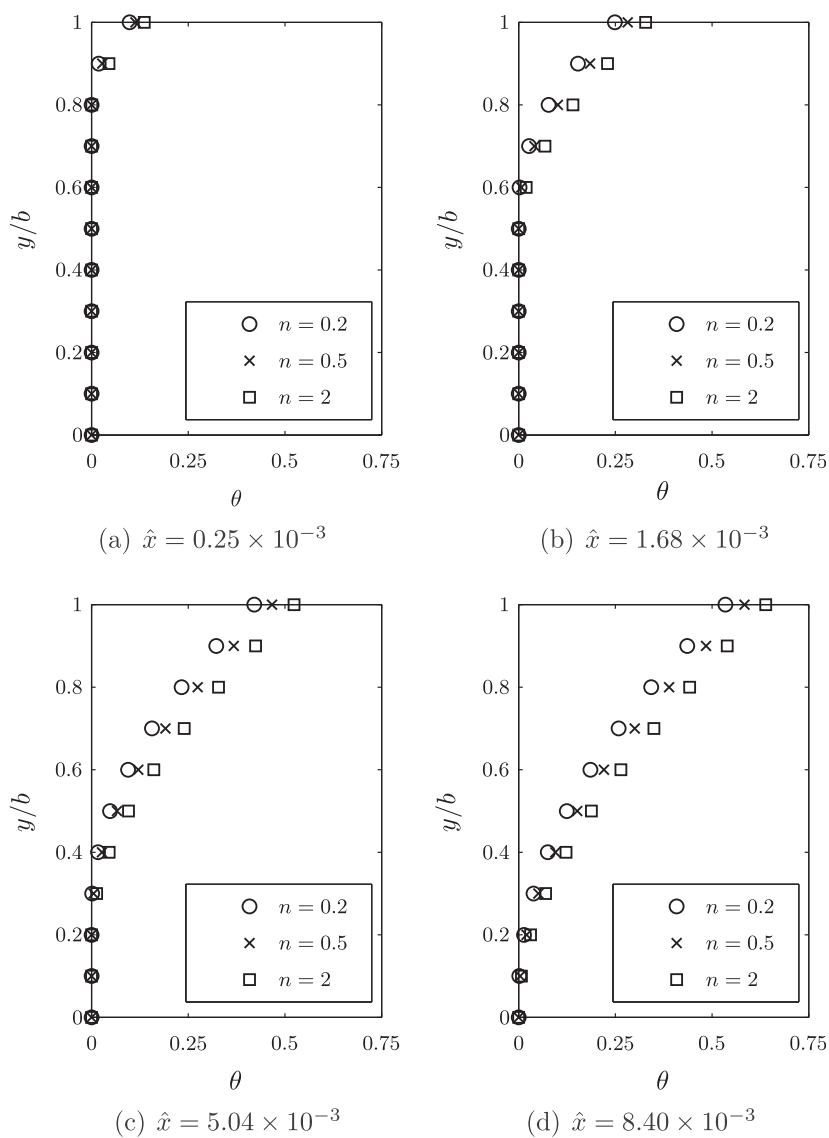
(d) $\hat{x} = 8.40 \times 10^{-3}$

Fig. 17. Non-dimensional temperature profiles at four axial positions for $\delta = \delta_{th}$.

This last integral can be integrated analytically only if $n = 1, 0.5, 0.333, 0.25, \ldots, 1/N$ where N is an integer. The corresponding expression is

$$I'_{B2} = -\frac{n^2}{(n+1)(3n+1)} I_1^* \tag{25d}$$

The value of I_1^* is calculated by applying the following recurrent expression for $j = N + 2$ to $j = 1$ and noting that $I_{N+3}^* = 0$

$$I_j^* = \frac{n}{1+(3+j)n}\left(1 - \frac{\Delta_{th}}{b}\right)^j - \frac{1+(2-j)n}{1+(3+j)n} I_{j+1}^* \tag{25e}$$

For other values of n the integral I'_{B2} must be evaluated numerically.

This general solution for the thermally developing flow is applied to the special case with $n = 1$ in order to compare its predictions with the corresponding results for Newtonian fluids obtained by Sparrow et al. [3]. Their expression for the non-dimensional temperature distribution (after adjustment to account for the difference in its definition from the present one) is

$$\theta(\hat{x}, y) = \frac{3}{4}\left(\frac{y}{b}\right)^2 - \frac{1}{8}\left(\frac{y}{b}\right)^4 + 16\left(\hat{x} - \frac{39}{4480}\right) + H(\hat{x}, y/b) \tag{26a}$$

where

$$H(\hat{x}, y/b) = \sum_1^\infty C_N Y_N\left(\frac{y}{b}\right) \exp(-(32/3)\hat{x}\beta_N^2) \tag{26b}$$

It must be noted that values of the eigenfunctions Y_N are only available for $y = b$ [4]. Therefore this expression can only be used to obtain the wall temperature and the Nusselt number (since the bulk temperature is again given by Eq. (20)).

It is interesting to note that the constant 39/4480 is the value of the non-dimensional thermal entrance length predicted by Eq. (23) for $n = 1$. However, this does not prove that it is also the value of $\hat{L}_{th}$ according to the solution by Sparrow et al. [3]. For this to be true the value of $H(\hat{x} = 39/4480, y)$ must be zero and the temperature at $\hat{x} = 39/4480$ calculated by Eq. (26) must be identical to that predicted by the exact analytical expression (Eq. (21d)). However, $H(\hat{x} = 39/4480, y = 1)$ is not zero (it is -0.040) and the non-dimensional wall temperature predicted by Eq. (26) is approximately 6.5% lower than the corresponding one predicted by Eq. (21d). These observations suggest that according to the solution by Sparrow et al. [3] the non-dimensional thermal entrance length is slightly higher than $39/4480 (\approx 0.0087)$. Indeed, the value of this parameter given in [4] is 0.0115439.

Further comparisons of the present solution with that by Sparrow et al. [3] are presented in Figs. 11 and 12. Fig. 11 shows that the present estimates of the wall temperature are everywhere somewhat higher than the corresponding predictions from [3]. The biggest difference occurs at $\hat{x} = 0.008705$ where our value is 6.9% higher. The asymptote shown in Fig. 11 corresponds to the constant temperature gradient in the developed region (see Eq. (14b)). Fig. 12 shows that the present estimates of the Nusselt number are always somewhat lower. The biggest difference occurs at $\hat{x} = 0.008705$ where our value is 8.3% lower. As a conclusion of these comparisons it can be said that the differences between the predictions of the two models are not significant and do not invalidate the proposed approximate solution which has the advantage of being more general.

Figs. 13–15(b) illustrate some of the results for the hydrodynamically developed flow. Contrary to the case of slug flow these results depend on the flow behavior index. Thus Fig. 13 shows that the thermal boundary thickness increases with n. Fig. 14 shows the non-dimensional temperature profiles at four axial positions and indicates that at any given position this temperature increases

with n. Fig. 15a compares the axial evolution of the Nusselt number predicted by the present model with corresponding results by Cotta & Özişik [14] and provides further proof of their validity and precision. Finally, Fig. 15(b) shows the evolution of the Nusselt number (evaluated as explained at the end of Section 4.1) which decreases as n increases. The value of the Nusselt number in the developed region is $9.70, 8.76, 8.38, 7.90$ and 7.59 for a flow behavior index of $0.2, 0.5, 0.8, 2$ and 10 respectively.

### 4.3. Simultaneously developing flow with $\delta(x) = \delta_{th}(x)$

As indicated by Shah & Bhatti [4] this equality is approached for fluids for which the Prandtl number is close to unity. It should be noted that the assumed equality between the hydrodynamic and thermal boundary layer thicknesses implies that $L_{hy} = L_{th}$.

In this case the velocity profile is given by Eqs. (5b), (5c) in the developed region and by Eqs. (6a), (6b), (7) in the developing region. The integral form of the momentum equation (Eq. (8)) as well as the expressions of the skin friction coefficient, Eqs. (12b) and (12c), are also valid. On the other hand, the Bernoulli equation (Eq. (9)) whose application has been questioned by Campbell & Slattery [15] is not used. Therefore Eqs. (10) and (11) which give the axial variation of the hydrodynamic boundary layer thickness and the hydrodynamic entrance length do not apply in this case.

Under these conditions the energy equation in the developed region, Eq. (14d), is identical to the corresponding expression for
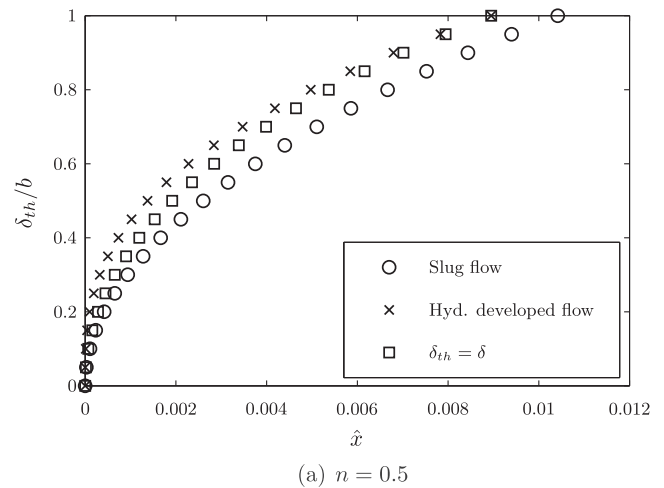
(a) $n = 0.5$
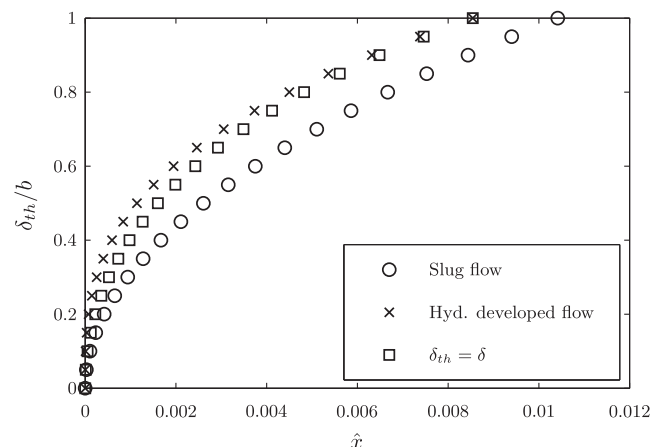
(b) $n = 2$

Fig. 19. Evolution of the boundary layer thickness for the three cases under study.

the case of hydrodynamically developed flow (Eq. (21a)). Therefore the temperature distribution in the developed region is again given by Eq. (21d) and as a consequence the corresponding temperature distribution in the developing region is again given by Eq. (22a) in the core and by Eq. (22b) in the boundary layer. Hence the expression for $L_{hy} = L_{th}$, obtained by applying the energy equation between $x = 0$ and $x = L_{hy} = L_{th}$ (Eq. (18a)), is again given by Eq. (23).

The only difference in the thermal fields between the present case and the one treated in Section 4.2 is the relation between the boundary layer thickness and the axial position which is obtained as before by applying the integral form of the energy equation between $x = 0$ and $x < L_{th}$ (Eq. (19a)). It is due to the difference between the corresponding velocity distributions which in the present case depends on both space coordinates while in the previous one it is independent of the axial position. The result of the integration of Eq. (19a) for the present case is

$$\hat{x} = \frac{(\delta/b)^2}{1 - \frac{n}{2n+1}(\delta/b)} \times \frac{(n+1)(24n^2 + 13n + 2)}{96(3n+1)(4n+1)(5n+2)} \quad (27)$$

Figs. 16–18 illustrate some of the results for the present case. As in the case of hydrodynamically developed flow and contrary to the case of slug flow the results for the present case depend on the flow behavior index. Fig. 16 shows that the boundary layer develops faster as this index increases. Therefore for a given value of $\hat{x}$ the boundary layer thickness increases with n while the entrance length decreases as n increases. The values of $L_{hy} = L_{th}$ are $0.009385, 0.008951, 0.008775, 0.008543$ and 0.008380 for $n = 0.2, 0.5, 0.8, 2$ and 10 respectively. Fig. 17 shows the non-dimensional temperature profiles at four axial positions in the developing region. It indicates the transition between the core region where $T(x, y) = T_0$, or equivalently $\theta = 0$, and the boundary layer. It also illustrates the fact that at any given position within the boundary layer the non-dimensional temperature increases with the flow behavior index. Finally, Fig. 18 shows the evolution of the Nusselt number for different values of the flow behavior index. As usual Nu decreases rapidly as $\hat{x}$ increases. As the flow behavior index increases the value of Nu decreases. Its values in the developed region are $9.70, 8.76, 8.38, 7.90$ and 7.59 (the same as in the hydrodynamically developed case) for $n = 0.2, 0.5, 0.8, 2$ and 10 respectively.

(a) $n = 0.5$, $\hat{x} = 2.1 \times 10^{-3}$

(b) $n = 0.5$, $\hat{x} = 6.7 \times 10^{-3}$

(c) $n = 2$, $\hat{x} = 2.1 \times 10^{-3}$

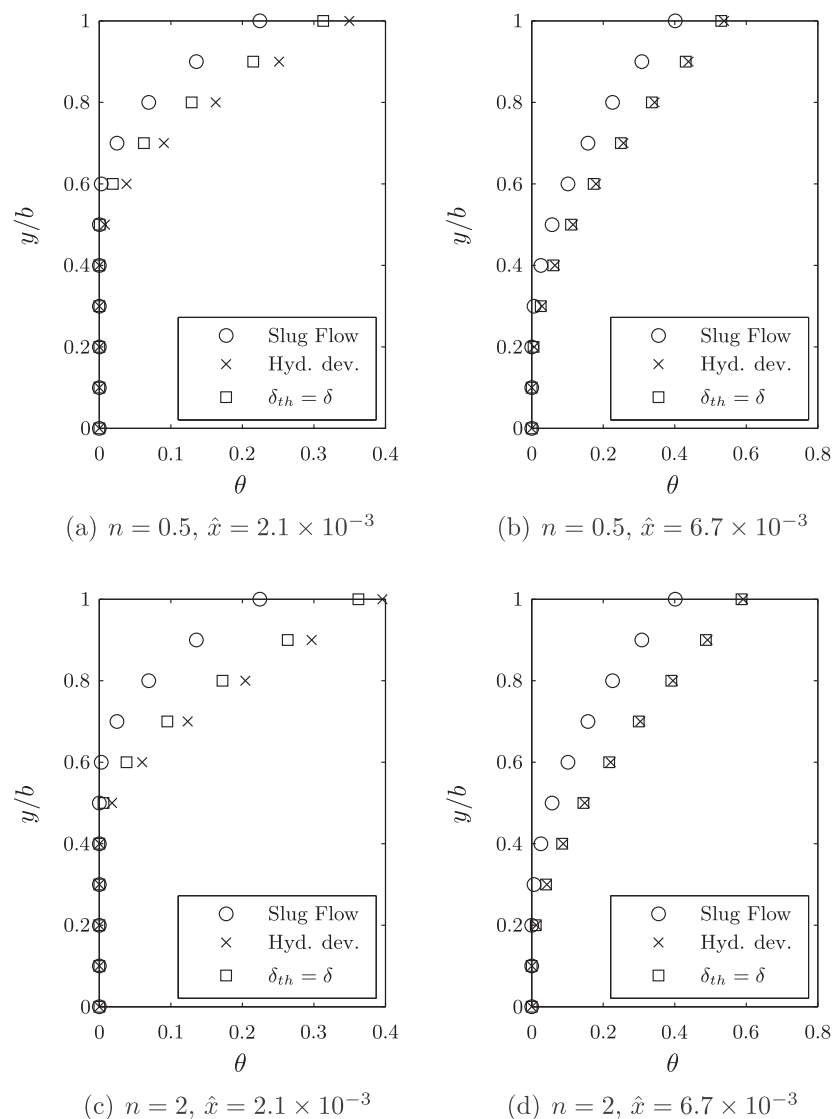(d) $n = 2$, $\hat{x} = 6.7 \times 10^{-3}$

Fig. 20. Comparison of temperature profiles for the three cases under study.

5. Comparisons between the different thermal cases

Fig. 19 compares the evolution of the thermal boundary layer thickness predicted by the three cases presented in Section 4 for two values of the flow behavior index. It shows that at a given axial position its value is smallest in the case of slug flow. As a result the corresponding thermal entrance length is the longest. On the other hand the thermal boundary layer grows faster for hydrodynamically developed flow than for flow with $\delta_{th} = \delta$ even though these two cases have the same thermal entrance length. These observations are valid for both values of the flow behavior index. The reason why δ_{th} is smallest in the case of slug flow is due to the fact that in this case the velocity near the walls is highest; therefore a greater fraction of the heat added from the walls is in this case convected downstream and the fraction contributing to the local temperature increase is the smallest. On the other hand, in the case of hydrodynamically developed flow the hydrodynamic boundary layer in the thermal entrance region is thicker than in the case with $\delta_{th} = \delta$; therefore in the case of hydrodynamically developed flow the fraction of the heat added from the walls which is convected downstream is smaller and as a result the fraction contributing to the local temperature increase is greatest.

Fig. 20 compares the corresponding temperature profiles at two axial positions for two values of the flow behavior index and confirms the arguments presented in the previous paragraph. It shows that for both values of n and at both axial positions the temperature of the fluid is lowest in the case of slug flow and highest in the case of hydrodynamically developed flow (the latter is more obvious at $\hat{x} = 2.1 \times 10^{-3}$, i.e. close to the inlet, but is also true at $\hat{x} = 6.7 \times 10^{-3}$). These observations confirm the arguments regarding the fraction of the heat added from the walls which contributes to the increase of the local fluid temperature.

6. Conclusion

The proposed approximate analytical solution of the flow of power-law fluids in the entrance region of parallel-plates ducts provides relatively simple algebraic expressions for the velocity distribution, for the boundary layer thickness, for the hydrodynamic entrance length, for the pressure loss and for the skin friction coefficient in terms of the flow behavior index and the space coordinates. It gives good estimates of the velocity and hydrodynamic entrance length in the special case of a flow behavior index equal to unity (Newtonian fluid).

The thermal problem in the same geometry with the H condition has been solved for three special cases: slug flow, hydrodynamically developed flow and flow with equal boundary layer thicknesses for the hydrodynamic and thermal fields. It provides relatively simple algebraic expressions for the temperature distribution, for the boundary layer thickness and for the Nusselt number in terms of the flow behavior index and the space coordinates. It gives good estimates of the Nusselt number and the thermal entrance length in the special case of a flow behavior index equal to unity (Newtonian fluid).

Conflict of interest

None.

References

[1] J. Bodoia, J.F. Osterle, Finite difference analysis of plane Poiseuille and Couette flow developments, Appl. Sci. Res. 10 (1961) 265–276, http://dx.doi.org/10.1007/BF00411919.
[2] M.S. Bhatti, C.W. Savery, Heat transfer in the entrance region of a straight channel: laminar flow with uniform wall heat flux, J. Heat Transf. 99 (1977) 142–144, http://dx.doi.org/10.1115/1.3450640.
[3] E.M. Sparrow, J.L. Novotny, S.H. Lin, Laminar flow of a heat-generating fluid in a parallel-plate channel, AIChE J. 9 (1963) 797–804, http://dx.doi.org/10.1002/aic.690090618.
[4] R.K. Shah, M.S. Bhatti, Laminar convective heat transfer in ducts, in: S. Kakac, R.K. Shah, W. Aung (Eds.), Handbook of Single-Phase Convective Heat transfer, 1997.
[5] C.L. Hwang, L.T. Fan, Finite difference analysis of forced convection heat transfer in entrance region of a flat rectangular duct, Appl. Sci. Res. A13 (1964) 401–422, http://dx.doi.org/10.1007/BF00382066.
[6] J. Yau, C. Tien, Simultaneous development of velocity and temperature profiles for laminar flow of a non-Newtonian fluid in the entrance region of flat ducts, Can. J. Chem. Eng. 41 (1963) 139–145, http://dx.doi.org/10.1002/cjce.5450410402.
[7] S. Richardson, Extended leveque solutions for flows of power law fluids in pipes and channels, Int. J. Heat Mass Transf. 22 (10) (1979) 1417–1423, http://dx.doi.org/10.1016/0017-9310(79)90204-7.
[8] Z. Matras, Z. Nowak, Laminar entry length problem for power-law fluids, Acta Mech. 48 (1983) 81–90, http://dx.doi.org/10.1007/BF01178498.
[9] R.M. Cotta, M.N. Özişik, Laminar forced convection of power-law non-Newtonian fluids inside ducts, Wärme Stoffübertrag. 20 (3) (1986) 211–218, http://dx.doi.org/10.1007/BF01303453.
[10] R. Magno, J. Quaresma, E. Macedo, Integral transform solution for the internal boundary layer of non-Newtonian fluids, Hybrid Methods Eng. 1 (1999) 173–184, http://dx.doi.org/10.1615/HybMethEng.v1.i2.60.
[11] R. Magno, E. Macedo, J. Quaresma, Solutions for the internal boundary layer equations in simultaneously developing flow of power-law fluids within parallel plates channels, Chem. Eng. J. 87 (2002) 339–350, http://dx.doi.org/10.1016/S1385-8947(01)00302-3.
[12] R.C. Gupta, On developing laminar non-Newtonian flow in pipes and channels, Nonlin. Anal.: Real World Appl. 2 (2001) 171–193, http://dx.doi.org/10.1016/S0362-546X(00)00109-7.
[13] N. Galanis, M. Rashidi, Entropy generation in non-Newtonian fluids due to heat and mass transfer in the entrance region of ducts, Heat Mass Transf. 48 (9) (2012) 1647–1662, http://dx.doi.org/10.1007/s00231-012-1009-7.
[14] R.M. Cotta, M.N. Özişik, Laminar forced convection to non-Newtonian fluids in ducts with prescribed wall heat flux, Int. Commun. Heat Mass Transf. 13 (3) (1986) 325–334, http://dx.doi.org/10.1016/0735-1933(86)90020-5.
[15] W. Campbell, J. Slattery, Flow in the entrance of a tube, J. Basic Eng. 85 (1963) 41–45, http://dx.doi.org/10.1115/1.3656529.
[16] K. Khellaf, G. Lauriat, A new analytical solution for heat transfer in the entrance region of ducts: hydrodynamically developed flows of power-law fluids with constant wall temperature, Int. J. Heat Mass Transf. 40 (1997) 3443–3447, http://dx.doi.org/10.1016/S0017-9310(96)00333-X.